文章编号:1672-6553-2024-22(8)-032-010

DOI:10.6052/1672-6553-2024-028

具有初始几何缺陷轴向运动 GPLRMF 圆锥壳的内共振行为研究*

丁浩轩　佘桂林†

(重庆大学 机械与运载工程学院，重庆　400044)

摘要　普遍认为，初始几何缺陷对结构非线性动力学行为具有重要影响. 然而，初始几何缺陷对轴向运动圆锥壳非线性内共振行为的影响机理尚不清楚. 为了回答这一问题，本文研究了具有初始几何缺陷和轴向运动的石墨烯片增强泡沫金属(GPLRMF)圆锥壳的 1∶2 内共振行为. 首先，基于 Reddy 高阶剪切变形理论和 von-Karman 几何非线性，导出了圆锥壳的运动控制方程. 然后，考虑前两阶振动模态，利用伽辽金原理对运动方程进行离散. 随后，采用多尺度法进行求解，通过数值计算得到前两种振动模态下圆锥壳的内共振动力学响应曲线. 最后，利用龙格－库塔法研究了在 1∶2 内共振条件下的运动分岔和混沌动力学行为.

关键词　非线性振动，　内共振，　圆锥壳，　分岔与混沌，　初始几何缺陷

中图分类号:O327　　**文献标志码**:A

Internal Resonances of Axially Moving GPLRMF Conical Shells with Initial Geometric Imperfection*

Ding Haoxuan　She Guilin†

(College of Mechanical and Vehicle Engineering, Chongqing University, Chongqing　400044)

Abstract　It is generally believed that initial geometric imperfection has a significant impact on the nonlinear dynamic behavior of structures. However, the mechanism that the initial geometric imperfection affects the nonlinear internal resonance behavior of axially moving conical shells is still unclear. To answer this question, the 1∶2 internal resonance behavior of graphene platelets reinforced metal foam (GPLRMF) conical shells with initial geometric imperfection and axial motion is studied in this paper. Firstly, based on the Reddy high-order shear deformation theory and von Karman geometric nonlinearity, the motion equation of the conical shell is derived. Then, considering the first two vibration modes and discretizing the motion equation through the Galerkin principle. Subsequently, the multi-scale method is used for solving, and the internal resonance dynamic response curves of the conical shell under the first two vibration modes are obtained through numerical calculations. Finally, the motion bifurcation and chaotic dynamic behavior under 1∶2 internal resonance conditions are studied using the Runge-Kutta method.

Key words　nonlinear vibration, internal resonance, conical shell, bifurcation and chaos, initial geometric imperfection

2024-03-07 收到第 1 稿，2024-03-27 收到修改稿.

* 重庆大学人才引进项目(02090011044159)，湖南省自然科学基金项目资助(2024JJ7466)，Chongqing University Talent Introduction Project (02090011044159), Hunan Provincial Natural Science Foundation of China (2024JJ7466).

† 通信作者 E-mail:sheguilin@cqu.edu.cn

引言

圆锥壳作为一种典型的工程结构,被广泛应用于航空航天等领域[1]. 在服役的过程中,圆锥壳不可避免地会产生共振问题,从而影响结构的正常运行,甚至引发灾难性的事故[2,3]. 目前,有关圆锥壳结构的屈曲[4-6]、自振[7,8]、共振[9-11]、分岔和混沌动力学[12-14]问题广为研究. 然而,尚无文献报道初始几何缺陷对圆锥壳内共振行为的影响.

实际上,圆锥壳结构在生产、制造和使用过程中,不可避免地会存在各种缺陷. 研究表明[15],即便是微小的缺陷,也会降低结构的承载能力,甚至影响结构的安全性和可靠性. Chen 等[15]研究了初始几何缺陷功能梯度板的自振特性. 考虑初始几何缺陷和轴向运动,Ding 和 She[10]研究了圆柱壳的主共振行为. 近年来,GPLRMF 作为一种优异的增强材料,由于轻量化、高刚度、高强度,已经引起了许多学者的广泛关注[16-18].

文献检索表明,现有关于轴向运动锥壳内共振行为的研究仅限于完美结构,忽略了初始几何缺陷的影响. 为了解决这一问题,本文首次研究了具有几何缺陷轴向运动圆锥壳结构的 1∶2 内共振行为. 利用 Reddy 高阶剪切变形理论,建立非线性动力学模型. 针对前两阶振动模态,使用多尺度法和龙格-库塔法求解运动方程. 最后,分别讨论了不同因素对内共振、分岔和混沌动力学行为的影响.

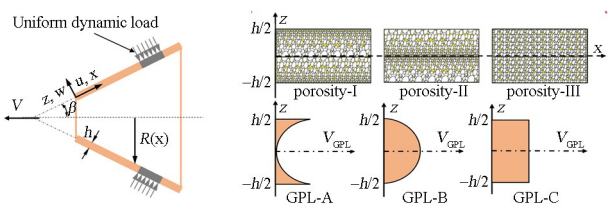

图 1　锥壳和材料分布类型

Fig. 1　A sketch of the conical shell and material distribution types

1　材料参数

考虑 Porosity-Ⅰ、Porosity-Ⅱ 和 Porosity -Ⅲ 三种不同的孔隙分布类型,且弹性模量与孔隙率系数 $e_i(i=1,2,3)$ 密切相关,质量密度与质量孔隙率 $e_{mi}(i=1,2,3)$ 密切相关,具体表达式如下[10],

$$E(z)=\begin{cases}E^{*}\left[1-e_1(1-\mathbb{N})\right],(\text{Porosity-Ⅰ})\\ E^{*}\{1-e_2\mathbb{N}\},(\text{Porosity-Ⅱ})\\ E^{*}e_3,(\text{Porosity-Ⅲ})\end{cases}$$

$$\rho(z)=\begin{cases}\rho^{*}\left[1-e_{m1}(1-\mathbb{N})\right],(\text{Porosity-Ⅰ})\\ \rho^{*}\{1-e_{m2}\mathbb{N}\},(\text{Porosity-Ⅱ})\\ \rho^{*}e_{m3},(\text{Porosity-Ⅲ})\end{cases}$$

$$\mu(z)=\mu^{*} \tag{1}$$

其中,$\mathbb{N}=1-\cos(\pi z/h)$,$E^{*}$,$\rho^{*}$ 和 μ^{*} 的定义与文献[10]一致,且[10]

$$E^{*}=\frac{3}{8}\left(\frac{1+\zeta_{\mathrm{L}}^{\mathrm{GPL}}\eta_{\mathrm{L}}^{\mathrm{GPL}}V_{\mathrm{GPL}}}{1-\eta_{\mathrm{L}}^{\mathrm{GPL}}V_{\mathrm{GPL}}}\right)\times E_{\mathrm{M}}+\frac{5}{8}\left(\frac{1+\zeta_{\mathrm{W}}^{\mathrm{GPL}}\eta_{\mathrm{W}}^{\mathrm{GPL}}V_{\mathrm{GPL}}}{1-\eta_{\mathrm{W}}^{\mathrm{GPL}}V_{\mathrm{GPL}}}\right)\times E_{\mathrm{M}}$$

$$\rho^{*}=\rho_{\mathrm{M}}(1-V_{\mathrm{GPL}})+\rho_{\mathrm{GPL}}V_{\mathrm{GPL}}$$

$$\mu^{*}=\mu_{\mathrm{M}}(1-V_{\mathrm{GPL}})+\mu_{\mathrm{GPL}}V_{\mathrm{GPL}} \tag{2}$$

$$V_{\mathrm{GPL}}=\begin{cases}Si_1\mathbb{N},(\text{GPL-A})\\ Si_2(1-\mathbb{N}),(\text{GPL-B})\\ Si_3,(\text{GPL-C})\end{cases} \tag{3}$$

弹性模量和密度之间的关系可以描述如下,

$$E(z)/E^{*}=[\rho(z)/\rho^{*}]^2 \tag{4}$$

把式(1)代入式中(4),从而得到,

$$\begin{cases}\sqrt{1-e_1(1-\mathbb{N})}=1-e_{m1}(1-\mathbb{N})\\ \sqrt{1-e_2\mathbb{N}}=1-e_{m2}\mathbb{N}\\ \sqrt{e_3}=e_{m3}\end{cases} \tag{5}$$

另外,在计算过程中还需要使用以下关系式,

$$\int_0^{\frac{h}{2}}\sqrt{1-e_1(1-\mathbb{N})}\,\mathrm{d}z=\int_0^{\frac{h}{2}}\sqrt{1-e_2\mathbb{N}}\,\mathrm{d}z=\int_0^{\frac{h}{2}}\sqrt{e_3}\,\mathrm{d}z \tag{6}$$

2　振动方程

根据 Reddy 高阶剪切变形壳理论,锥壳中任意点的位移分量可以描述为:

$$U_1(x,\theta,z,t)=u_0(x,\theta,t)+z\varphi_x+c_1z^3\left(\varphi_x+\frac{\partial w_0}{\partial x}\right) \tag{7}$$

$$U_2(x,\theta,z,t)=v_0(x,\theta,t)+z\varphi_y+c_1z^3\left(\varphi_y+\frac{1}{R}\frac{\partial w_0}{\partial\theta}\right) \tag{8}$$

$$U_3(x,\theta,t)=w_0(x,\theta,t) \tag{9}$$

其中,$c_1=4/3h^2$,$c_2=3c_1$.

考虑初始几何缺陷时,方程(9)应改写为:

$$U_3(x,\theta,t)=w_0(x,\theta,t)+w_1(x,\theta) \tag{10}$$

考虑到几何非线性,几何方程可以表示为:

$$\varepsilon_{xx}=\varepsilon_{xx}^{0}+z\kappa_{xx}^{1}+z^{3}\kappa_{xx}^{3},\quad \eta_{xy}=\eta_{xy}^{0}+z\eta_{xy}^{1}+z^{3}\eta_{xy}^{3},$$
$$\varepsilon_{yy}=\varepsilon_{yy}^{0}+z\kappa_{yy}^{1}+z^{3}\kappa_{yy}^{3},\quad \eta_{xz}=\eta_{xz}^{0}+z^{2}\eta_{xz}^{2},\eta_{yz}=\eta_{yz}^{0}+z^{2}\eta_{yz}^{2}\tag{11}$$

其中，$\begin{pmatrix}\varepsilon_{xx}^{0}\\ \varepsilon_{yy}^{0}\\ \eta_{xy}^{0}\end{pmatrix}=\begin{Bmatrix}\dfrac{\partial u_0}{\partial x}+\dfrac{1}{2}\left(\dfrac{\partial w_0}{\partial x}\right)^2+\dfrac{\partial w_0}{\partial x}\dfrac{\partial w_1}{\partial x}\\ \dfrac{1}{R}\dfrac{\partial v_0}{\partial\theta}+\dfrac{w_0}{R}\cos\beta+\dfrac{1}{2}\dfrac{1}{R^2}\left(\dfrac{\partial w_0}{\partial\theta}\right)^2+\dfrac{1}{R^2}\dfrac{\partial w_0}{\partial\theta}\dfrac{\partial w_1}{\partial\theta}+\dfrac{u_0}{R}\sin\beta\\ \dfrac{1}{R}\dfrac{\partial u_0}{\partial\theta}+\dfrac{\partial v_0}{\partial x}-\dfrac{v_0}{R}\sin\beta+\dfrac{1}{R}\dfrac{\partial w_0}{\partial x}\dfrac{\partial w_0}{\partial\theta}+\dfrac{1}{R}\dfrac{\partial w_0}{\partial x}\dfrac{\partial w_1}{\partial\theta}+\dfrac{1}{R}\dfrac{\partial w_1}{\partial x}\dfrac{\partial w_0}{\partial\theta}\end{Bmatrix}$，

$$\begin{pmatrix}\kappa_{xx}^{1}\\ \kappa_{yy}^{1}\\ \eta_{xy}^{1}\end{pmatrix}=\begin{Bmatrix}\dfrac{\partial\varphi_x}{\partial x}\\ \dfrac{1}{R}\dfrac{\partial\varphi_y}{\partial\theta}+\dfrac{1}{R}\varphi_x\sin\beta\\ \dfrac{1}{R}\dfrac{\partial\varphi_x}{\partial\theta}+\dfrac{\partial\varphi_y}{\partial x}-\dfrac{1}{R}\varphi_y\sin\beta\end{Bmatrix},\ \begin{pmatrix}\eta_{xz}^{0}\\ \eta_{yz}^{0}\end{pmatrix}=\begin{Bmatrix}\varphi_x+\dfrac{\partial w_0}{\partial x}\\ \varphi_y+\dfrac{1}{R}\dfrac{\partial w_0}{\partial\theta}-\dfrac{1}{R}v_0\cos\beta\end{Bmatrix},$$

$$\begin{pmatrix}\kappa_{xx}^{3}\\ \kappa_{yy}^{3}\\ \eta_{xy}^{3}\end{pmatrix}=c_1\begin{pmatrix}\kappa_{xx}^{1}\\ \kappa_{yy}^{1}\\ \eta_{xy}^{1}\end{pmatrix},\ \begin{pmatrix}\eta_{xz}^{2}\\ \eta_{yz}^{2}\end{pmatrix}=c_2\begin{pmatrix}\eta_{xz}^{0}\\ \eta_{yz}^{0}\end{pmatrix}\tag{12}$$

利用 Hamilton 原理导出了如下运动方程：

$$\frac{\partial N_{xx}}{\partial x}+\frac{1}{R}\frac{\partial N_{xy}}{\partial\theta}+\frac{N_{xx}}{R}\sin\beta-\frac{N_{yy}}{R}\sin\beta=\overline{I_1}\left(\frac{\partial^2u}{\partial t^2}+2V_c\frac{\partial^2u}{\partial x\partial t}+V_c^2\frac{\partial^2u}{\partial x^2}\right)+\overline{I_2}\frac{\partial^2\psi_x}{\partial t^2}-c_1\overline{I_3}\frac{\partial^3w}{\partial x\partial t^2},$$
$$\frac{\partial N_{xy}}{\partial x}+\frac{1}{R}\frac{\partial N_{yy}}{\partial\theta}+\frac{2N_{xy}}{R}\sin\beta+\frac{S_{yy}}{R}\cos\beta=\overline{I_1^*}\left(\frac{\partial^2v}{\partial t^2}+2V_c\frac{\partial^2v}{\partial x\partial t}+V_c^2\frac{\partial^2v}{\partial x^2}\right)+\overline{I_2^*}\frac{\partial^2\psi_y}{\partial t^2}-c_1\overline{I_3^*}\frac{1}{R}\frac{\partial^3w}{\partial\theta\partial t^2},$$
$$\frac{\partial S_{xx}}{\partial x}+\frac{1}{R}\frac{\partial S_{yy}}{\partial\theta}+\frac{S_{xx}}{R}\sin\beta-\frac{N_{yy}}{R}\cos\beta+c_2\left(\frac{\partial C_{xx}}{\partial x}+\frac{1}{R}\frac{\partial C_{yy}}{\partial\theta}\right)+N_{yy}\frac{1}{R^2}\frac{\partial^2w}{\partial\theta^2}+c_1\left(\frac{\partial^2K_{xx}}{\partial x^2}+\frac{2}{R}\frac{\partial^2K_{xy}}{\partial x\partial\theta}+\right.$$
$$\left.\frac{1}{R^2}\frac{\partial^2K_{yy}}{\partial\theta^2}\right)+\frac{N_{yy}}{R}+N_{xx}\frac{\partial^2w}{\partial x^2}+\frac{N_{xx}}{R}\frac{\partial w}{\partial x}\sin\beta+\frac{2}{R}N_{xy}\frac{\partial^2w}{\partial x\partial\theta}-P\frac{\partial^2w}{\partial x^2}+\overline{\lambda_q}\cos(\Omega t)=$$
$$I_1\left(\frac{\partial^2w}{\partial t^2}+2V_c\frac{\partial^2w}{\partial x\partial t}+V_c^2\frac{\partial^2w}{\partial x^2}\right)+C_t\left(\frac{\partial w}{\partial t}+V_c\frac{\partial w}{\partial x}\right)+\overline{I_3}\frac{\partial^3u}{\partial x\partial t^2}+\overline{I_3^*}\frac{1}{R}\frac{\partial^3v}{\partial\theta\partial t^2}+c_1\overline{I_5}\frac{\partial^3\psi_x}{\partial x\partial t^2}+$$
$$c_1\overline{I_5^*}\frac{1}{R}\frac{\partial^3\psi_y}{\partial\theta\partial t^2}-c_1^2I_7\left(\frac{\partial^4w}{\partial x^2\partial t^2}+\frac{1}{R^2}\frac{\partial^4w}{\partial\theta^2\partial t^2}\right),$$
$$\frac{\partial M_{xx}}{\partial x}+\frac{1}{R}\frac{\partial M_{xy}}{\partial\theta}-S_{xx}+c_2C_{xx}-c_1\left(\frac{\partial K_{xx}}{\partial x}+\frac{1}{R}\frac{\partial K_{xy}}{\partial\theta}\right)=\overline{I_2}\frac{\partial^2u}{\partial t^2}+\overline{I_4}\frac{\partial^2\psi_x}{\partial t^2}-\overline{I_5}\frac{\partial^3w}{\partial x\partial t^2},$$
$$\frac{\partial M_{xy}}{\partial x}+\frac{1}{R}\frac{\partial M_{yy}}{\partial\theta}-S_{yy}+c_2C_{yy}-c_1\left(\frac{\partial K_{xy}}{\partial x}+\frac{1}{R}\frac{\partial K_{yy}}{\partial\theta}\right)=\overline{I_2^*}\frac{\partial^2v}{\partial t^2}+\overline{I_4^*}\frac{\partial^2\psi_y}{\partial t^2}-\overline{I_5^*}\frac{1}{R}\frac{\partial^3w}{\partial\theta\partial t^2}\tag{13}$$

方程(13)中惯性矩的定义与文献[14]一致.

3 求解方法

由于锥壳内共振行为主要受前两阶模态的影响，因此采用如下位移场型函数[13,14]

$$u_0=U_1(t)\cos\left(\frac{\pi m_1x}{L}\right)\sin(n_1\theta)+U_2(t)\cos\left(\frac{\pi m_2x}{L}\right)\sin(n_2\theta)\tag{14}$$

$$v_0=V_1(t)\sin\left(\frac{\pi m_1x}{L}\right)\cos(n_1\theta)+V_2(t)\sin\left(\frac{\pi m_2x}{L}\right)\cos(n_2\theta)\tag{15}$$

$$w_0=W_1(t)\sin\left(\frac{\pi m_1x}{L}\right)\sin(n_1\theta)+W_2(t)\sin\left(\frac{\pi m_2x}{L}\right)\sin(n_2\theta)\tag{16}$$

$$w_1=W_{11}(t)\sin\left(\frac{\pi m_1x}{L}\right)\sin(n_1\theta)+W_{22}(t)\sin\left(\frac{\pi m_2x}{L}\right)\sin(n_2\theta)\tag{17}$$

$$\varphi_x=\varphi_{x1}(t)\cos\left(\frac{\pi m_1x}{L}\right)\sin(n_1\theta)+$$

$$\varphi_{x2}(t)\cos\left(\frac{\pi m_2 x}{L}\right)\sin(n_2\theta) \tag{18}$$

$$\varphi_y=\varphi_{y1}(t)\sin\left(\frac{\pi m_1 x}{L}\right)\cos(n_1\theta)+\varphi_{y2}(t)\sin\left(\frac{\pi m_2 x}{L}\right)\cos(n_2\theta) \tag{19}$$

其中，$U_1(t)$,$U_2(t)$,$V_1(t)$,$V_2(t)$,$W_1(t)$,$W_2(t)$,$\varphi x_1(t)$,$\varphi y_2(t)$ 是振动幅值. 同时，引入以下无量纲量：

$$\overline{W}_1=\frac{W_1}{h},\overline{W}_2=\frac{W_2}{h},\overline{\Omega}_1=\frac{\Omega_1}{\omega_1},\tau=t\omega_1,$$

$$\overline{F}_{ij}=\frac{F_{ij}}{\omega_1^2},(i=1,2,\ j=1,2),$$

$$\overline{F}_{ik}=\frac{F_{ik}h}{\omega_1^2},(i=1,2,\ k=5,6,7),$$

$$\overline{F}_{il}=\frac{F_{il}h^2}{\omega_1^2},(i=1,2,\ l=3,4,8,9),$$

$$\overline{F}_{io}=\frac{F_{io}}{h\omega_1^2},(i=1,2,\ o=10) \tag{20}$$

其中，ω_1 表示圆锥壳的一阶固有频率，经过一系列的运算，可以得到无量纲的常微分方程组，

$$\ddot{\overline{W}}_1(\tau)+\mu_1\dot{\overline{W}}_1(\tau)+\overline{F}_{11}\overline{W}_1(\tau)+\overline{F}_{12}\overline{W}_2(\tau)+\overline{F}_{13}\overline{W}_1^3(\tau)+\overline{F}_{14}\overline{W}_1^2(\tau)\overline{W}_2(\tau)+\overline{F}_{15}\overline{W}_1^2(\tau)+\overline{F}_{16}\overline{W}_1(\tau)\overline{W}_2(\tau)+\overline{F}_{17}\overline{W}_2^2(\tau)+\overline{F}_{18}\overline{W}_1(\tau)\overline{W}_2^2(\tau)+\overline{F}_{19}\overline{W}_2^3(\tau)=\overline{F}_{110}\overline{F}_1\cos(\overline{\Omega}_1\tau) \tag{21}$$

$$\ddot{\overline{W}}_2(\tau)+\mu_2\dot{\overline{W}}_2(\tau)+\overline{F}_{21}\overline{W}_1(\tau)+\overline{F}_{22}\overline{W}_2(\tau)+\overline{F}_{23}\overline{W}_1^3(\tau)+\overline{F}_{24}\overline{W}_1^2(\tau)\overline{W}_2(\tau)+\overline{F}_{25}\overline{W}_1^2(\tau)+\overline{F}_{26}\overline{W}_1(\tau)\overline{W}_2(\tau)+\overline{F}_{27}\overline{W}_2^2(\tau)+\overline{F}_{28}\overline{W}_1(\tau)\overline{W}_2^2(\tau)+\overline{F}_{29}\overline{W}_2^3(\tau)=\overline{F}_{210}\overline{F}_2\cos(\overline{\Omega}_1\tau) \tag{22}$$

在式(21)、式(22)中，W_1 和 W_2 分别是前两阶振动模态下的横向振动幅值，μ_1 和 μ_2 表示阻尼系数，F_1 和 F_2 表示一阶和二阶振动模态下外激励的幅值，Ω_1 表示外激励频率. 使用多尺度法开展摄动分析. 因此，式(21)和(22)可以进一步写为，

$$\ddot{\overline{W}}_1(\tau)+\varepsilon\mu_1\dot{\overline{W}}_1(\tau)+\overline{F}_{11}\overline{W}_1(\tau)+\overline{F}_{12}\overline{W}_2(\tau)+\varepsilon\overline{F}_{13}\overline{W}_1^3(\tau)+\varepsilon\overline{F}_{14}\overline{W}_1^2(\tau)\overline{W}_2(\tau)+\varepsilon\overline{F}_{15}\overline{W}_1^2(\tau)+\varepsilon\overline{F}_{16}\overline{W}_1(\tau)\overline{W}_2(\tau)+\varepsilon\overline{F}_{17}\overline{W}_2^2(\tau)+\varepsilon\overline{F}_{18}\overline{W}_1(\tau)\overline{W}_2^2(\tau)+\varepsilon\overline{F}_{19}\overline{W}_2^3(\tau)=\varepsilon\overline{F}_{110}\overline{F}_1\cos(\overline{\Omega}_1\tau) \tag{23}$$

$$\ddot{\overline{W}}_2(\tau)+\varepsilon\mu_2\dot{\overline{W}}_2(\tau)+\overline{F}_{21}\overline{W}_1(\tau)+\overline{F}_{22}\overline{W}_2(\tau)+\varepsilon\overline{F}_{23}\overline{W}_1^3(\tau)+\varepsilon\overline{F}_{24}\overline{W}_1^2(\tau)\overline{W}_2(\tau)+\varepsilon\overline{F}_{25}\overline{W}_1^2(\tau)+\varepsilon\overline{F}_{26}\overline{W}_1(\tau)\overline{W}_2(\tau)+\varepsilon\overline{F}_{27}\overline{W}_2^2(\tau)+\varepsilon\overline{F}_{28}\overline{W}_1(\tau)\overline{W}_2^2(\tau)+\varepsilon\overline{F}_{29}\overline{W}_2^3(\tau)=\varepsilon\overline{F}_{210}\overline{F}_2\cos(\overline{\Omega}_1\tau) \tag{24}$$

其中，ε 是摄动小参数. 考虑 1∶2 内共振并引入失谐参数 σ_1 和 σ_2，随后利用多尺度法，经过一系列数学推导，可以得到式(23)和式(24)的最终渐近解，具体求解步骤可以参考 Yang 等[13,14].

4　数值分析

在开展参数研究之前，进行模型退化验证，具体结果见表 1 和图 2. 结果表明，当前结果与文献[18]～文献[20]一致，从而验证了本文的正确性.

表 1　与文献[19]、文献[20]的对照

Table 1　Comparison with refs. [19] and refs. [20]

n	本文	Shu [19]	Liew et al. [20]
1	0.811	0.812	0.812
2	0.669	0.669	0.669
3	0.542	0.542	0.542
4	0.456	0.456	0.456
5	0.408	0.408	0.408
6	0.395	0.396	0.396
7	0.413	0.414	0.414

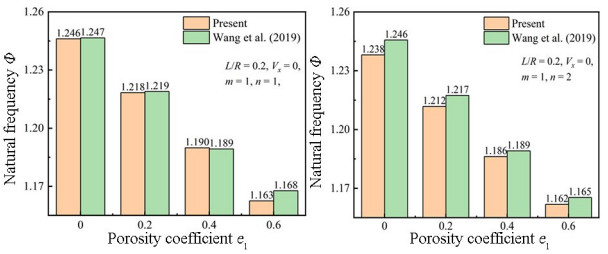

图 2　对比分析（$m=1,L/R=0.2,\rho_m=7850\text{kg/m}^3$，$\mu_m=0.3,V=0,\Phi=\Omega R\sqrt{\rho_m/E_m},E_m=200\text{GPa}$)

Fig. 2　Comparative analysis ($m=1,L/R=0.2,\rho_m=7850\text{kg/m}^3$, $\mu_m=0.3,V=0,\Phi=\Omega R\sqrt{\rho_m/E_m},E_m=200\text{GPa}$)

表 2　材料属性

Table 2　Material properties

几何尺寸和物理参数	锥壳	GPLs	基体
长度/m	0.2	2.5×10^{-6}	—
厚度/m	0.01	1.5×10^{-9}	—
宽度/m	—	1.5×10^{-6}	—
小径/m	0.2	—	—
杨氏模量/MPa	—	1010	200
泊松比	—	0.186	0.3
密度/(kg/m^3)	—	1060	7850

4.1 1∶2 内共振分析

在参数研究中,所采用的材料见表 2. 除非特别提及,其他参数的选择为:GPL-A, Porosity-Ⅰ, $W_{gpl}=1\%, e_1=0.2, L/R_1=1, R_1/h=20, F=2.5, \mu=0.6, V=0.05, W_1=0.02, \beta=45°$.

图 3(a)和图 3(b)研究了激振力和阻尼系数对 1∶2 内共振行为的影响. 可以看出内共振响应曲线

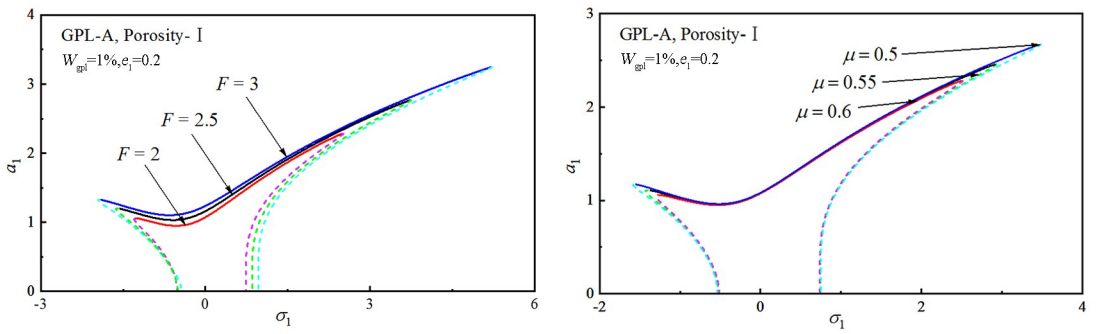

图 3 外部激励和阻尼系数的影响

Fig. 3 Influences of external excitation and damping coefficients

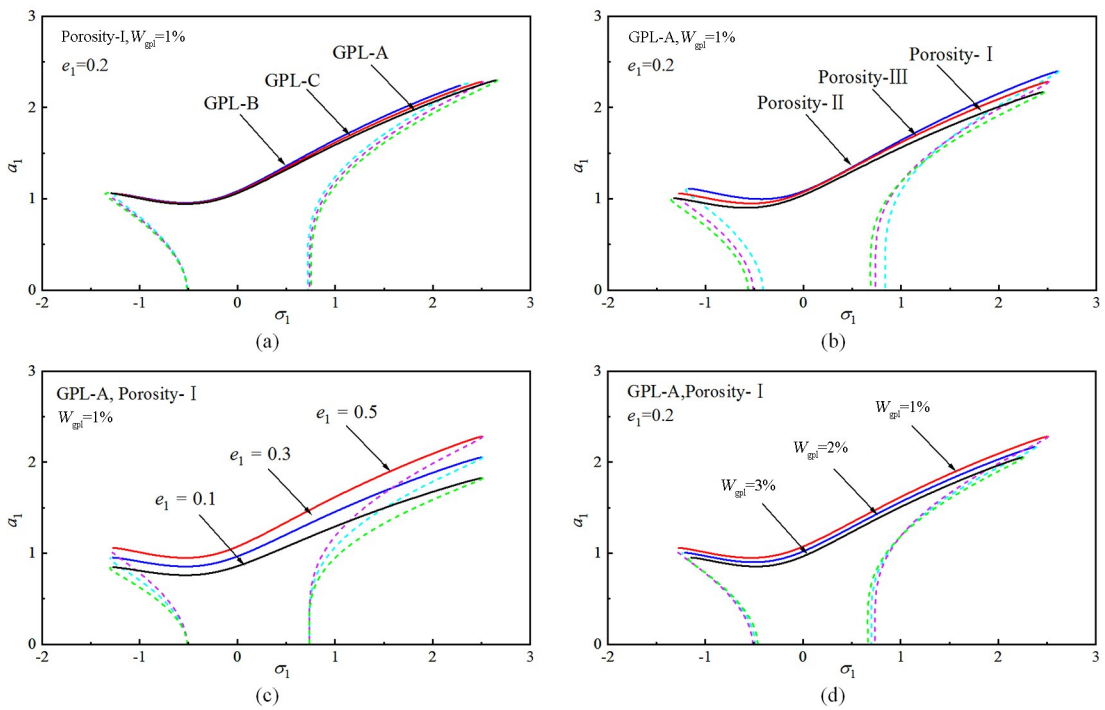

图 4 GPLs 分布类型、孔隙分布类型、孔隙系数和 GPLs 质量分数的影响

Fig. 4 The influences of GPLs distribution types, porosity distribution types, porosity coefficient, and GPLs mass fraction

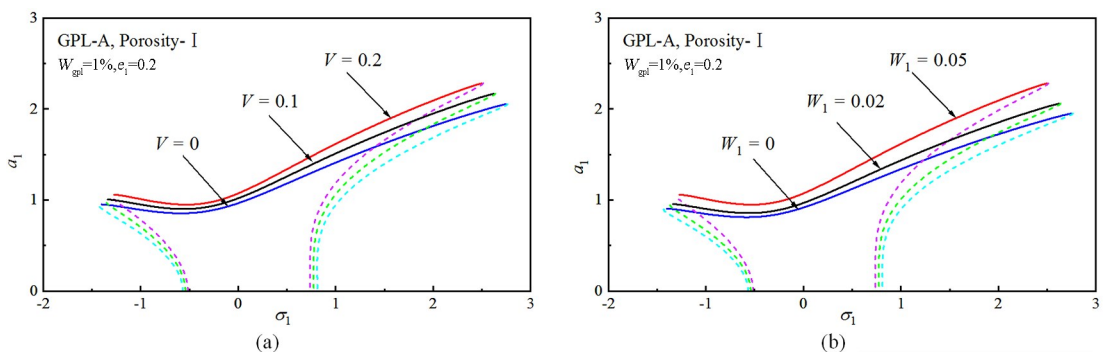

图 5 轴向速度和几何缺陷的影响

Fig. 5 Effects of axial velocity and geometrical imperfections

存在双跳跃现象. 当 σ_1 接近某个特征值时,锥壳的振幅会发生急剧变化,且激振力越大,振幅越大,共振域越大. 阻尼越大,振幅越小,共振域越小.

图 4 研究了材料参数的影响. 可以看出,GPLs 分布类型对内共振问题没有显著影响;孔隙-I 锥壳的振幅最小,孔隙-II 锥壳的振幅最大;随着孔隙系数的增加,振幅逐渐增大,随着 GPLs 质量分数的增加,幅度逐渐减小.

图 5 中分别研究了轴向速度和初始几何缺陷的影响. 从中可以看出,随着轴向速度或初始几何缺陷的增加,振幅逐渐增大,共振域减小.

4.2　分岔和混沌分析

在本节中,考虑 1∶2 内共振条件,初始条件被假定为:$Y_{10}=-0.34$, $X_{10}=0.19$, $Y_{20}=0.41$, $X_{20}=-0.23$.

从图 6 可以看出,随着外激励 F 的增加,其运动状态依次呈现出混沌(点 A)、单周期运动(点 B)和混沌(点 C)的现象,这意味着外部激励过大或过小都会导致系统呈现混沌状态,图 6(a)和图 6(b)有相同的运动趋势,但一阶振动模态下的振幅更大.

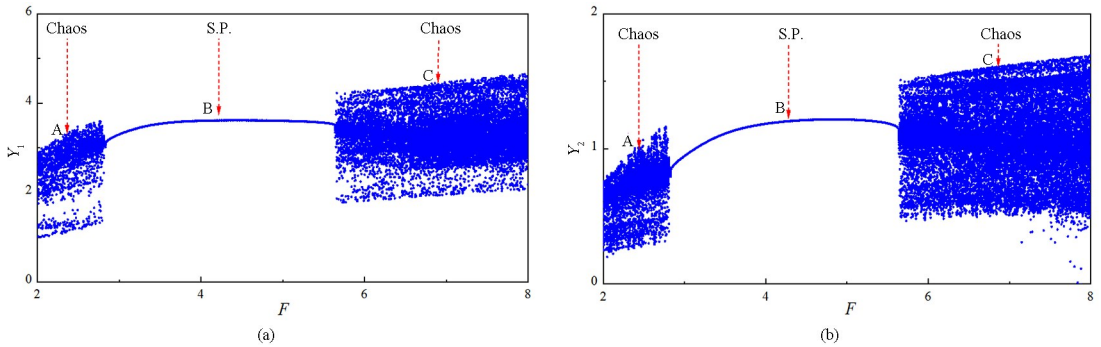

图 6　不同外部激励下的分岔曲线

Fig. 6　Bifurcation under different external excitation

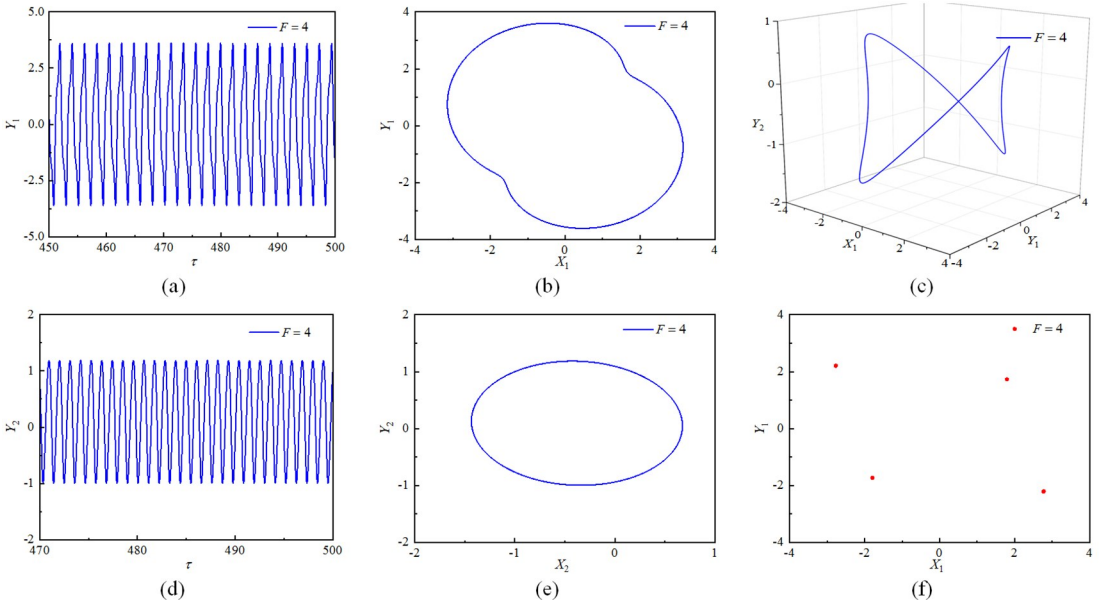

图 7　当 $F=4$ 时,时程历程图、相轨迹和庞加莱截面

Fig. 7　Time history diagram, phase trajectory and Poincare interface at $F=4$

图 7 和图 8 分别研究了在 $F=4$ 和 $F=6$ 时的时间历程、相轨迹和庞加莱截面. 显然,当 $F=4$ 时,系统表现出单一的周期性运动,时间历程图表现出稳定的周期运动,其相轨迹投影呈现出稳定环,其庞加莱截面有四个点. 相反,系统在 $F=6$ 时表现出混沌状态,系统的最大振幅是不稳定的,庞加莱截面上密集地布满了斑块,表明运动状态是混沌的.

从图 9 中可以看出,对于一阶模态,随着迟滞系数 σ_1 的增加,系统呈现出单周期(A点)－双周

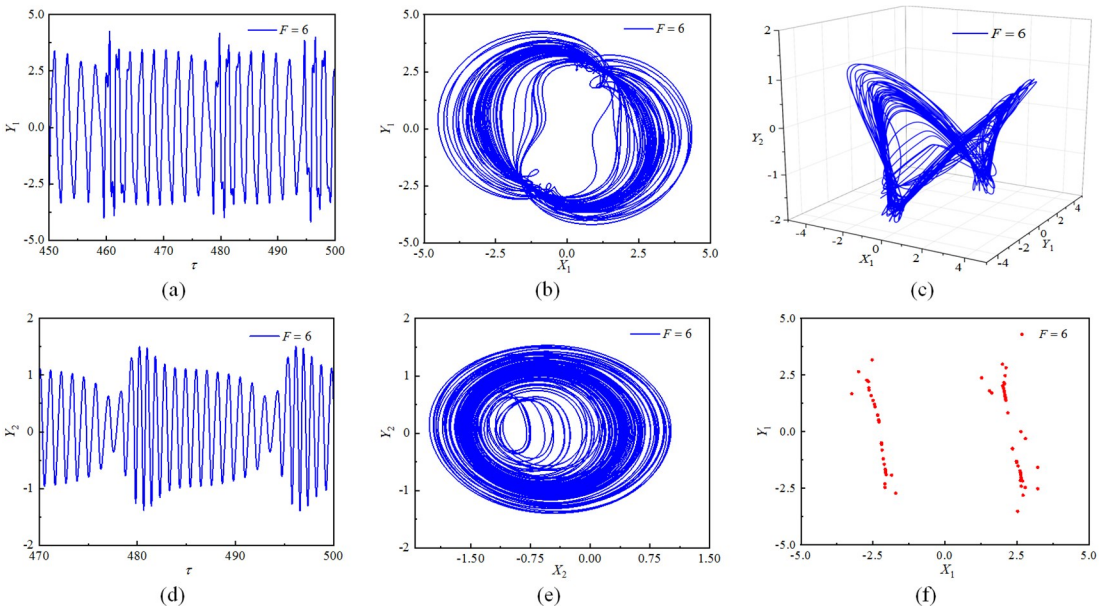

图 8 $F=6$ 时程历程图、相轨迹和庞加莱截面

Fig. 8 Time history diagram, phase trajectory and Poincare interface at $F=6$

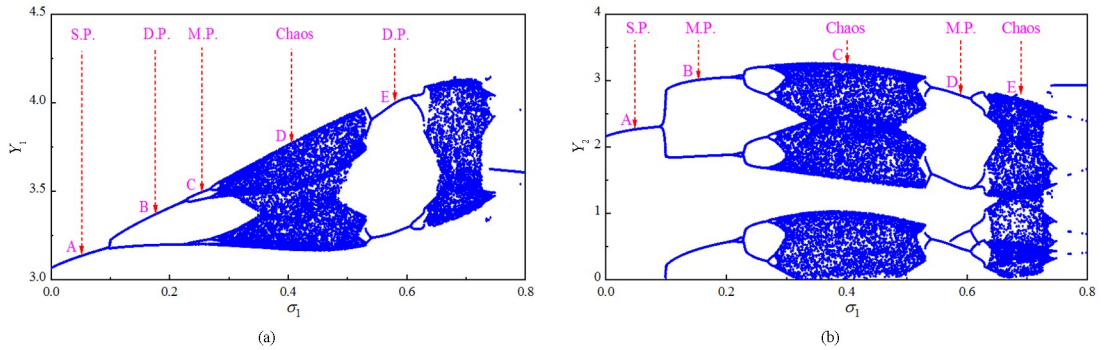

图 9 不同失谐参数下的分岔曲线 σ_1

Fig. 9 Bifurcation phenomenon under different σ_1

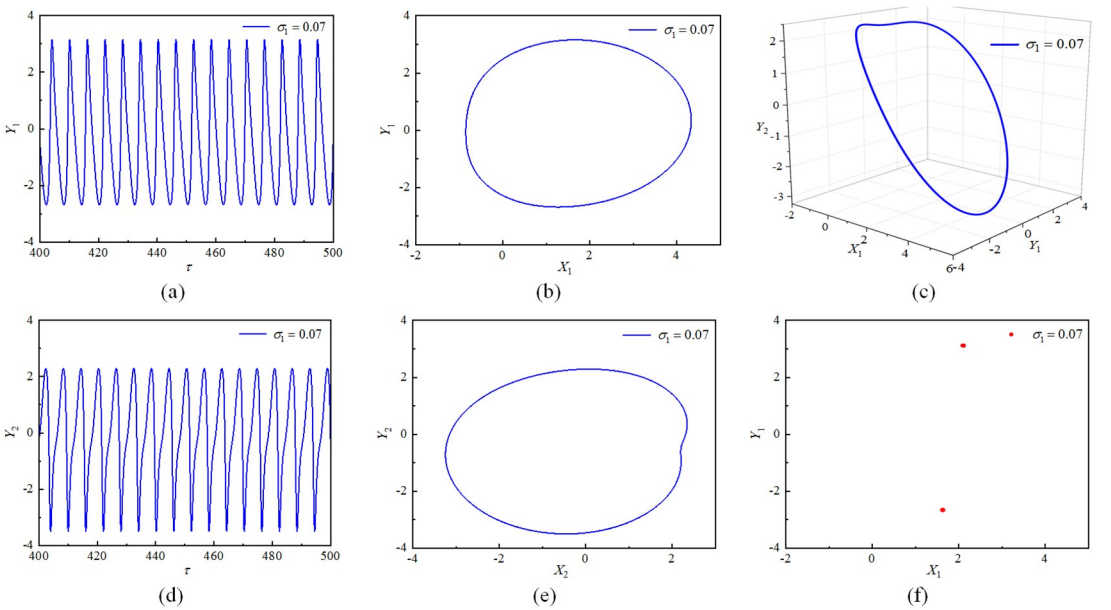

图 10 当 $\sigma_1=0.07$ 时，时间历程图、相轨迹和庞加莱截面

Fig. 10 Time history diagram, phase trajectory and Poincare interface at $\sigma_1=0.07$

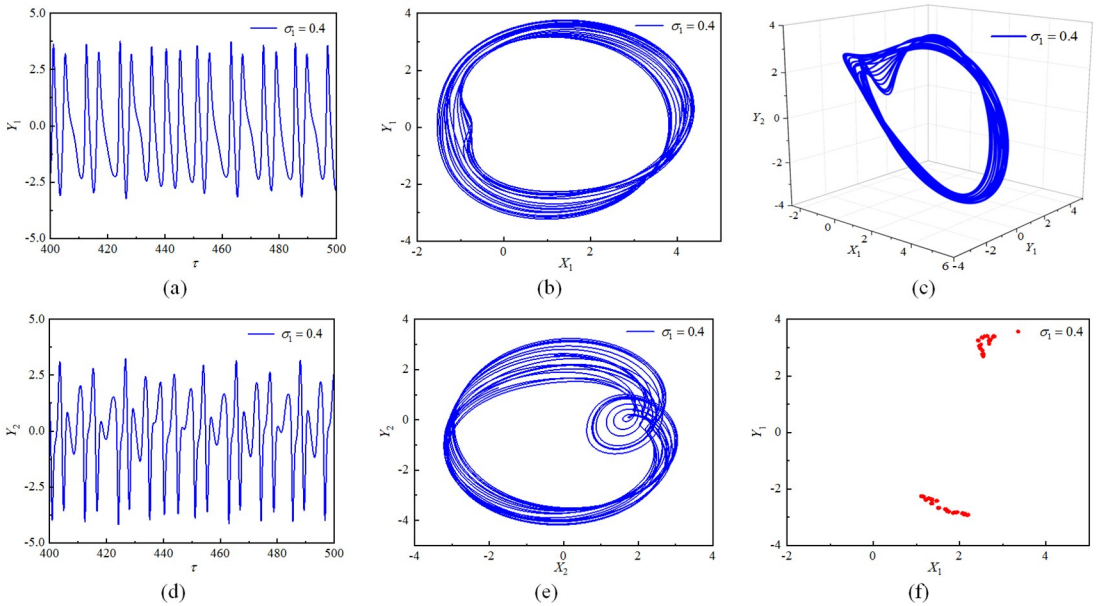

图 11　当 $\sigma_1=0.4$ 时,时间历程图、相轨迹和庞加莱截面

Fig. 11　Time history diagram, phase trajectory and Poincare interface at $\sigma_1=0.4$

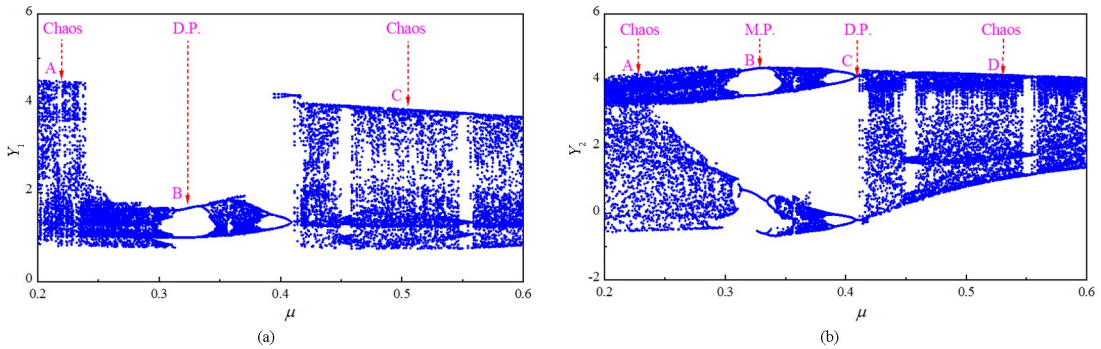

图 12　轴向运动壳体在不同阻尼系数下的分岔曲线

Fig. 12　Bifurcation phenomenon of axially moving shell under different damping coefficients

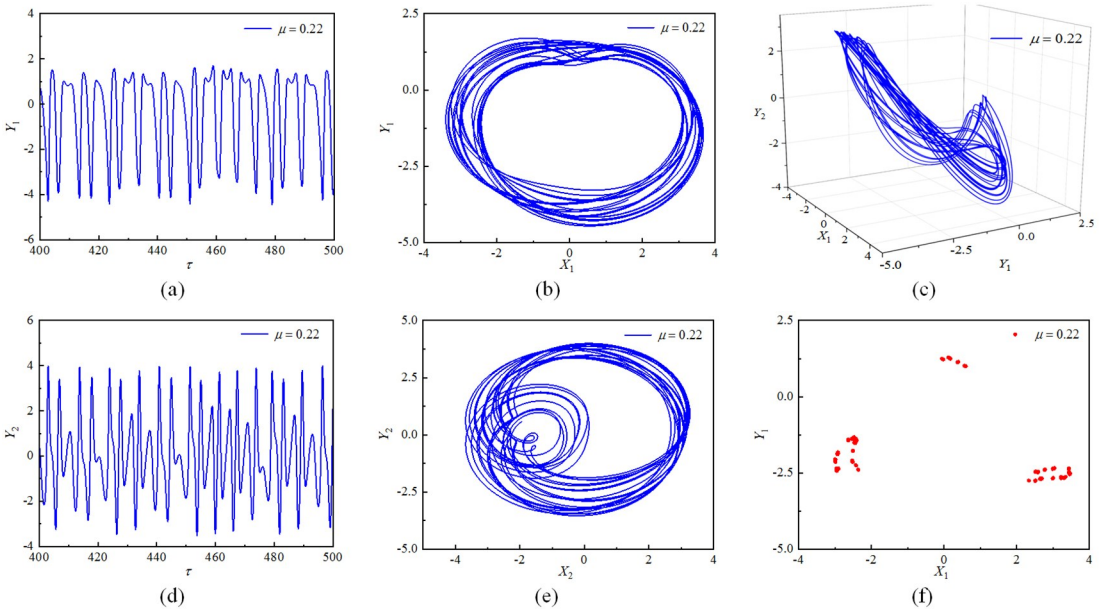

图 13　当 $\mu=0.22$ 时,时间历程图、相轨迹和庞加莱截面

Fig. 13　Time history diagram, phase trajectory and Poincare interface at $\mu=0.22$

期(B 点)—多周期(C 点)—混沌(D 点)—双周期　　(E 点)的运动趋势. 相反,对于二阶模态,系统经历

了单周期(点 A)－多周期(点 B)－混沌(点 C)－多周期(点 D)－混沌(点 E)的过程. 这表明,当 σ_1 一定时,一阶和二阶振动模态下的圆锥壳可能表现出不同的运动状态,这与图 6 所示的现象不同.

在图 10 中,锥壳在第一阶和第二阶振动模态下都表现出单一的周期性运动. 时间历程图和相轨迹相对稳定,庞加莱截面只有两点,可以确定运动状态是周期性的. 当 $\sigma_1=0.4$ 时(图 11),运动形式都呈现出混沌运动.

图 12 研究了阻尼系数的影响. 对于一阶振动模态,随着阻尼系数的增加,系统大致呈现混沌(A 点)－单周期(B 点)－混沌(C 点)运动状态. 然而,二阶振动模态呈现出与一阶振动模态不同的运动状态,系统呈现出的运动趋势依次是混沌(A 点)－多周期(B 点)－单周期(C 点)－混沌(D 点). 从图 13 中可以看出,当阻尼系数 u=0.22 时,圆锥壳呈现出明显的混沌现象.

5 总结

本文研究了具有初始几何缺陷和轴向运动的石墨烯片增强金属泡沫圆柱壳的 1∶2 内共振行为,利用 Galerkin 原理对前两阶模态的运动方程进行离散化处理. 然后,采用多尺度法求解控制方程,得到了前两阶模态的内共振响应曲线. 最后,利用龙格－库塔法对控制方程进行数值求解,获得了 1∶2 内共振条件下圆锥壳结构的动态响应,研究了系统的分岔与混沌现象,得到的结论如下:

(1)轴向运动速度对圆锥壳的 1∶2 内共振行为有显著影响,较高的轴向速度可能导致结构不稳定.

(2)在 1∶2 内共振条件下,初始几何缺陷的存在会使圆锥壳的振幅增大,导致结构失稳.

(3)材料参数可以改变圆锥壳的刚度,从而影响 1∶2 内共振行为.

(4)在 1∶2 内共振条件下,外力、阻尼和迟滞系数显著影响圆锥壳结构的分岔和混沌行为.

参考文献

[1] WANG A W, PANG Y Q, ZHANG W, et al. Nonlinear dynamic analysis of functionally graded graphene reinforced composite truncated conical shells [J]. International Journal of Bifurcation and Chaos, 2019, 29(11): 1950148.

[2] 吴先强, 赵珧冰, 郭智锐, 等. 温度变化对悬索全局动力学特性影响 [J]. 动力学与控制学报, 2023, 21(4): 32－40.
WU X Q, ZHAO Y B, GUO Z R, et al. Influences of temperature changes on global dynamical characteristics of suspended cables [J]. Journal of Dynamics and Control, 2023, 21(4): 32－40. (in Chinese)

[3] JAMSHIDI R, JAFARI A A. Nonlinear vibration of conical shell with a piezoelectric sensor patch and a piezoelectric actuator patch [J]. Journal of Vibration and Control, 2022, 28(11/12): 1502－1519.

[4] 韩勤锴, 秦朝烨, 褚福磊. 周期轴向力作用下旋转圆锥薄壳动力稳定性研究 [J]. 动力学与控制学报, 2022, 20(4): 40－47.
HAN Q K, QIN Z Y, CHU F L. Dynamic stability of rotating thin conical shells under periodic axial force [J]. Journal of Dynamics and Control, 2022, 20(4): 40－47. (in Chinese)

[5] ZAREI M, RAHIMI G H. Buckling characteristics of sandwich conical shells with variable skin thickness [J]. International Journal of Applied Mechanics, 2021, 13(9): 2150100.

[6] LIU F, NIU T Y, GONG J G, et al. Experimental and numerical investigations on buckling behaviours of axially compressed cylindrical-conical-cylindrical shells at elevated temperature [J]. Thin-Walled Structures, 2023, 184: 110549.

[7] LIAN Y S, LI X, SUN J Y, et al. A semi-analytical method for free vibration of semi-closed shells of revolution with variable curvature [J]. Journal of Vibration and Control, 2023, 29(9/10): 2198－2213.

[8] GUO C C, LIU T, BIN Q, et al. Free vibration analysis of coupled structures of laminated composite conical, cylindrical and spherical shells based on the spectral-Tchebychev technique [J]. Composite Structures, 2022, 281: 114965.

[9] 揭晓博, 张伟. 双叶片整体叶盘的非线性振动分析 [J]. 动力学与控制学报, 2019, 17(2): 136－142.
JIE X B, ZHANG W. Nonlinear vibration analysis of blisk with two blades [J]. Journal of Dynamics and Control, 2019, 17(2): 136－142. (in Chinese)

[10] DING H X, SHE G L. Nonlinear primary resonance behavior of graphene platelet-reinforced metal foams conical shells under axial motion [J]. Nonlinear Dy-

namics, 2023, 111(15): 13723－13752.

[11] ZHANG Y H, LIU W G. Nonlinear vibration response of a functionally graded carbon nanotube-reinforced composite conical shell using a stress function method [J]. Acta Mechanica, 2022, 233(8): 3157－3174.

[12] ZHANG Y H, LIU W G, LYU Z P, et al. Analysis of nonlinear vibration response of a functionally graded truncated conical shell with piezoelectric layers [J]. Journal of Mechanical Science and Technology, 2022, 36(8): 3897－3909.

[13] YANG S W, HAO Y X, ZHANG W, et al. Nonlinear vibration of functionally graded graphene platelet-reinforced composite truncated conical shell using first-order shear deformation theory [J]. Applied Mathematics and Mechanics, 2021, 42(7): 981－998.

[14] YANG S W, ZHANG W, HAO Y X, et al. Nonlinear vibrations of FGM truncated conical shell under aerodynamics and in-plane force along meridian near internal resonances [J]. Thin-Walled Structures, 2019, 142: 369－391.

[15] CHEN X C, LU Y X, WU Z B, et al. Free vibration of in-plane bi-directional functionally graded materials rectangular plates with geometric imperfections and general elastic restraints [J]. Aerospace Science and Technology, 2023, 132: 108045.

[16] 张博, 郭翔鹰, 姜盼. 石墨烯树脂复合材料板 1∶3 内共振非线性动力学分析 [J]. 动力学与控制学报, 2020, 18(4): 44－51.
ZHANG B, GUO X Y, JIANG P. Nonlinear dynamic analysis of graphene resin composites plate-with 1∶3 internal resonance [J]. Journal of Dynamics and Control, 2020, 18(4): 44－51. (in Chinese)

[17] 郭宇红, 张伟, 杨晓东. 1∶1 内共振情况下轻质材料层合板动力学的奇异性分析 [J]. 动力学与控制学报, 2018, 16(1): 6－20.
GUO Y H, ZHANG W, YANG X D. Singularity analysis on dynamics of light-weight sandwichplate under 1∶1 resonance [J]. Journal of Dynamics and Control, 2018, 16(1): 6－20. (in Chinese)

[18] WANG Y Q, YE C, ZU J W. Nonlinear vibration of metal foam cylindrical shells reinforced with graphene platelets [J]. Aerospace Science and Technology, 2019, 85: 359－370.

[19] SHU C. An efficient approach for free vibration analysis of conical shells [J]. International Journal of Mechanical Sciences, 1996, 38(8/9): 935－949.

[20] LIEW K M, NG T Y, ZHAO X. Free vibration analysis of conical shells via the element-free kp-Ritz method [J]. Journal of Sound and Vibration, 2005, 281(3/4/5): 627－645.